Junctionless Silicon Nanowire Resonator

Sebastian T. Bartsch, Maren Arp, and Adrian M. Ionescu, *Member, IEEE*

***Abstract*—The development of nanoelectromechanical systems (NEMS) is likely to open up a broad spectrum of applications in science and technology. In this paper, we demonstrate a novel double-transduction principle for silicon nanowire resonators, which exploits the depletion charge modulation in a junctionless field effect transistor body and the piezoresistive modulation. A mechanical resonance at the very high frequency of 100 MHz is detected in the drain current of the highly doped silicon wire with a cross-section down to ∼30 nm. We show that the depletion charge modulation provides a ∼35 dB increase in output signal-to-noise compared to the second-order piezoresistive detection, which can be separately investigated within the same device. The proposed junctionless resonator stands, therefore, as a unique and valuable tool for comparing the field effect and the piezoresistive modulation efficiency in the same structure, depending on size and doping. The experimental frequency stability of 10 ppm translates into an estimated mass detection noise floor of ∼ 60 kDa at a few seconds integration time in high vacuum and at room temperature. Integrated with conventional semiconductor technology, this device offers new opportunities for NEMS-based sensor and signal processing systems hybridized with CMOS circuitry on a single chip.**

***Index Terms*—Field effect transistor, nanoelectromechanical systems, nanowires, NEMS, piezoresistance, resonator, resonant-body transistor, RF, sensors, silicon-on-insulator.**

I. INTRODUCTION

IN THE PAST decade, NEMS have been gaining increasing attention for their superb ability to detect mass and force on the atomic scale [1], [2], and to prove fundamental laws of quantum physics [3]. The development of NEMS sensors is likely to open up a broad spectrum of applications in science and technology and revolutionize a range of fields from mass spectrometry [4] to biomedical diagnostics [5]. In recent years, mechanical resonators have undergone a continuous reduction in dimensions, reaching molecular levels in the form of carbon nanotubes or graphene [6], [7]. One reason for this development is that NEMS, because of their inherent properties as mechanical sensors, tremendously benefit from size reduction [8]. The detection of mass and force in the zeptogram (10^{-21} g) - and attonewton (10^{-18} N) - range, respectively, has been demonstrated [1], [2], [4], [9], [10]. To unfold the full potential of these resonators, fabricating and controlling NEMS on a large scale that comprise tens of thousands of resonators, will be necessary. Large area technologies that enable the parallel processing of mass information have a great impact on the development in several fields, such as system biology, where the parallel operation of millions of FET-based sensors recently enabled non-optical genome sequencing on-chip [11]. In terms of NEMS, these requirements severely limit the choice of material and of the type of mechanical transducer. Silicon technology remains therefore a promising avenue to follow for NEMS-based systems targeting a high level of integration and complexity [12]. The piezoresistive effect in silicon has been proposed as displacement transducer compatible with electronic integration and scalable in frequency and size, and was implemented in a variety of mechanical designs [4], [10], [13], [14].

Manuscript received January 10, 2013; revised November 25, 2013; accepted December 11, 2013. Date of publication December 18, 2013; date of current version March 3, 2014. The review of this paper was arranged by Editor M. Anwar.

The authors are with the School of Engineering, Swiss Federal Institute of Technology, Lausanne 1015, Switzerland (e-mail: sebastian.bartsch@epfl.ch; maren.arp@student.kit.edu; adrian.ionescu@epfl.ch).

Color versions of one or more of the figures in this paper are available online at http://ieeexplore.ieee.org.

Digital Object Identifier 10.1109/JEDS.2013.2295246

II. PRINCIPLE OF OPERATION

In this study, we created electromechanical resonators in form of highly doped, suspended silicon nanowires that exploit the intrinsic gain in a junctionless FET to transduce mechanical motion up to 100 MHz on-chip. The junctionless FET as a digital switch has been proposed by Colinge *et al.* [15] suitable for addressing the scaling challenges of multigate (nanowire) transistors that arise in terms of engineering super-abrupt junction profiles for high performance FETs on nanometer-thin films. Such devices are highly doped and the ON-state is characterized by a conduction channel in the entire silicon body; by applying a gate bias, the conduction channel can be depleted, and eventually pinch-off the conduction path (OFF-state).

However, the junctionless FET has never been proposed as a scalable, electromechanical transducer. Here, a highly conductive channel in form of a silicon nanowire was freely suspended. We modulated its cross-section through the two depletion regions controlled by two lateral, air-gap gates. The ultra-small cross-section (sub-40 nm) of the nanowire made this modulation very effective. At the mechanical resonance, the depletion width varied, thereby modulating the drain current. Fig. 1 illustrates the principle of operation. This operation is in total contrast with the previously reported resonant-body and resonant-gate FET [16]–[19], where the carrier density in inversion or accumulation layers was modulated to create a low resistivity path in a high resistivity channel region.

In the linear region and in depletion mode, the drain current I_D and the transconductance g_m in a junctionless transistor consisting of a highly n-doped nanowire body with two lateral gates are approximated:

$$I_D = q\mu N_{si} \frac{t_{Si}\left[W_{Si} - 2W_{dep}\right]}{L} V_D \tag{1}$$

2168-6734 © 2013 IEEE. Translations and content mining are permitted for academic research only. Personal use is also permitted, but republication/redistribution requires IEEE permission. See http://www.ieee.org/publications_standards/publications/rights/index.html for more information

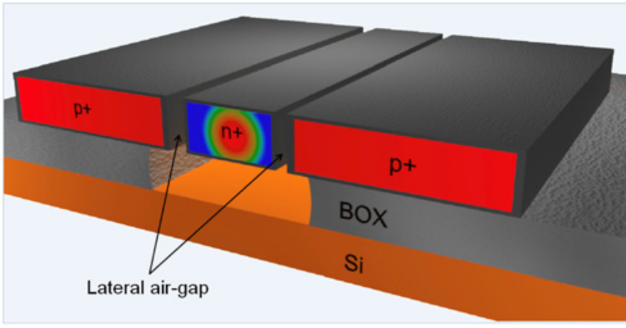

Fig. 1. **Schematic of a double-gate, junctionless silicon nanowire resonator.** The nanowire transistor is n + doped and freely suspended. The gate electrodes (p + doped) are separated *via* two air-gaps and control the depletion charge in the channel region. The color coding indicates high carrier densities in red, in the blue region the channel is fully depleted (zero density). At resonance, the lateral motion of the beam modulates the depletion charge, hence the drain current.

$$g_m = \frac{2\mu V_D}{L^2} C_g \quad (2)$$

where W_{Si} is the body (lateral) width, W_{dep} the depletion depth, N_{si} the channel doping concentration, μ the carrier mobility, t_{Si} the channel thickness, and L the channel lengths. The gate capacitance C_g is related to the depletion depth through $W_{dep} \approx - C_g\ V_G\ /\ (L\ t_{Si}\ q\ N_{Si})$.

The electromechanical current modulation due to the field effect is composed of (i) the modulation of the depletion charge that results from applying an a.c. voltage and maintaining a constant gap, and (ii) its modulation due to the time-varying gap under constant gate voltage. For an electrostatic actuation scheme based on a driven damped harmonic resonator model [6], [17], the field-effect current is then:

$$i_{FET} = \partial I_D \approx g_m \tilde{v}_g \left(1 + \frac{C_g'^2 V_G^2}{C_g m_{eff}} \frac{1}{\omega_0^2 - \omega_0 + i\omega\omega_0/Q} \right) \quad (3)$$

where C'_g the derivative of the gate capacitance with respect to the nanowire position, $\tilde{v}_g$ the a.c. voltage amplitude, and m_{eff} the resonator modal mass.

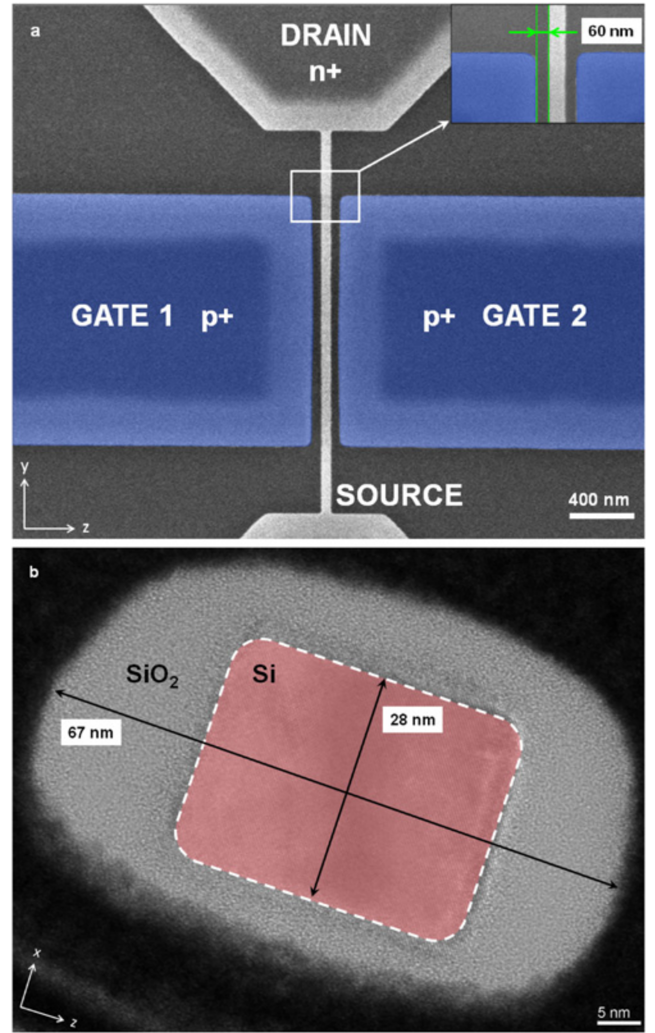

Fig. 2. **Integrated silicon-on-insulator junctionless nanowire resonators. a,** The scanning electron microscope image (top view) of a representative device (2.4 μm long). Electromechanical coupling is achieved through 60 nm lateral air-gap capacitors. The device layer is transparent and reveals the unreleased buried oxide underneath. The terminals and the doping configuration are indicated. **b,** The transmission electron microscope image of the nanowire, showing the silicon body surrounded by a thermally grown silicon oxide. The silicon body has a cross-section of $\sim$ 28 x 35 nm^2. The lattice planes in the single crystal silicon are visible.

III. Fabrication

The key to fabricating a junctionless NEM resonator is to form a suspended, crystalline silicon structure that is sufficiently thin to fully deplete the transistor channel via the action of the nearby gate electrode. We used a surface nanomachining process based on SOI-CMOS technology and 8" commercial SOI wafers. The 70 nm thick, silicon (100) layer was first thinned down to ~35 nm by sacrificial oxidation. The two ion implantations with phosphorus (n+) and boron (p+) defined the gate ($> 1 \times 10^{20}$ cm^{-3}) and the channel doping concentration ($\sim 2 \times 10^{18}$ cm^{-3}), respectively. The NEMS active area was patterned using hybrid DUV/e-beam lithography and anisotropic reactive ion etching. The nanowire resonators were oriented along the <110> crystal direction. After release of the 145 nm thick buried oxide, the resonators were terminated with a ~16 nm thermal oxide. The dielectric ensured a ultra-low leakage current, improved the electromechanical coupling and the gating effect. The fabrication and the co-integration with CMOS was similar to Ref. [20].

The junctionless architecture offered the advantage of enabling a self-aligned process, given that the gate electrodes are specific to the NEM resonator and simultaneously define the transistor channel. In order to address a single device on-chip, flexible 60 nm air-gap capacitors were used to couple the two independent gate electrodes to the nanowire resonator. The resonators had a typical length between 1 and 2.4 μm, a final height of 44 nm, and a final width of $\sim$ 67 nm (Fig. 2a). The width of the gate electrode was typically chosen 3/4 of the beam length. The resulting silicon body had a final cross-section of 28×35 nm^2 (Fig. 2b). Given the estimated maximum depletion depth of $W_{dep,max} \sim 25$ nm, the channel was fully depletable by the action of the two gate electrodes.

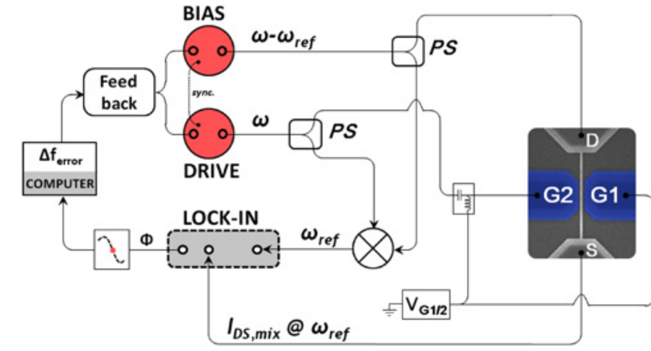

Fig. 3. **Schematic of the measurement circuit used for the actuation, detection and tracking of the mechanical resonance of the suspended channel, junctionless nanowire FET.** Shown is the closed-loop case; for open loop measurements, the feedback branch is interrupted. PS stands for power splitter, ° for the reference mixer. The two frequency sources are synchronized. The reference frequency is typically set < 10 kHz.

Higher channel doping concentrations are desirable and principally achievable; however, geometrical limits to obtain full depletion of the channel region were imposed by the minimum feature size achievable with this technology (about ∼ 45 nm).

IV. Characterization

The devices were measured in a vacuum-probe station by Cascade/Süss Microtech with RF GSG-probes (Süss Microtech) under high vacuum conditions (<1x10^{-5} mbar), using a lock-in detector SR-830 by Stanford Research and two RF signal sources HP8648D. The device performance as function of pressure was measured by flooding the chamber progressively with nitrogen and monitoring the pressure with a Pfeiffer PKR 251 and a SMC ZSE30 gauge, respectively. For DC measurements, an Agilent parametric analyzer 4556C was used with the same set-up.

The actuation, detection and tracking of the natural frequency of oscillation of the resonator were based on a heterodyne technique [6], [17]. The detection circuit offered two major benefits: first, the input and output frequencies were off-set by orders of magnitude, which suppressed the parasitic feed-through. Secondly, the output signal was mixed down to frequencies well below the cut-off frequency of the measurement system which resulted from the low-pass filter formed by the high device output impedance and the parasitic capacitances introduced by cables and contact pads. This method preserved therefore a large electromechanical signal-to-noise ratio (SNR). The schematic of the circuit is presented in Fig. 3. Shown is the closed-loop case; for open loop measurements, the feedback branch was interrupted. The two high frequency signals, which are denoted as *bias* and *drive*, were off-set by ω_{ref} and applied to the gate and the drain terminal, respectively. The transistor intrinsically acted as a resistive mixer ($V_D = 0$V) and down-converted the high frequency inputs to yield a low-frequency output current component $I_{DS,mix}$ at the difference frequency (<10 kHz). This drain current was recorded with a computer controlled lock-in amplifier as a function of the swept frequency (open loop time constant typically ∼30 ms). For closed-loop operation, we integrated our device into a digital feedback loop which tracked the resonance frequency in real-time [21]. The feedback signal was generated from the phase-frequency relation, which is linear around resonance and valid for the mechanical linear regime. From the constant phase condition, an error signal was computed (LabView) and fed back to correct the frequency of the signal generators. The sampling time was set typically ∼1s (shorter sampling times were principally limited by GPIB communication speed, ∼100 ms).

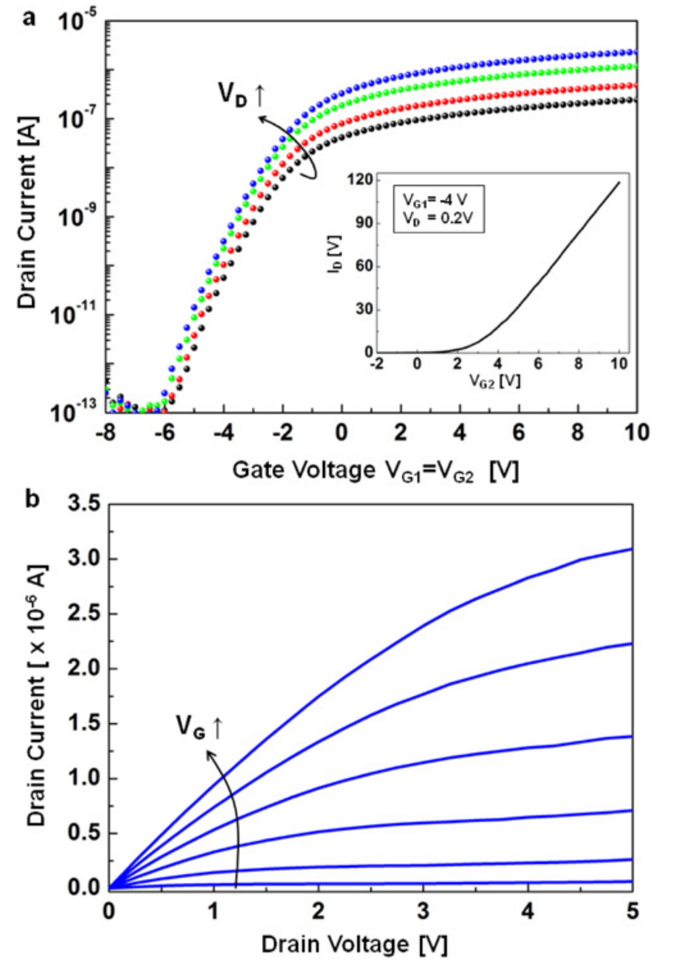

Fig. 4. **Full transistor tunability implemented in a nanoelectromechanical resonator. a,** Transfer characteristics of the 1.7 μm long nanowire resonator (log scale). The drain current versus gate voltage ($V_G = V_{G1} = V_{G2}$) for the drain voltages $V_D = 0.1$ V, 0.2 V, 0.5 and 1 V. The transfer curve shows off-currents corresponding to the noise floor of the measurement system (fA). The inset shows the transfer curve of the device when biased asymmetrically with a constant $V_{G1} = -4$V (linear scale), resulting in a threshold voltage of ∼ 3V. **b,** Drain current versus drain voltage for different (symmetric) gate voltages V_G showing linear and saturated operating regions. V_G is biased from -2V to + 3V in steps of 1V.

V. Results

A. *Static Characteristics*

In Fig. 4a-4b, we see the measured static characteristics of the suspended junctionless transistor with a well-behaved transition from the OFF- to the ON-state. In Fig. 4a, the drain current is plotted versus gate voltage. The transfer curve shows

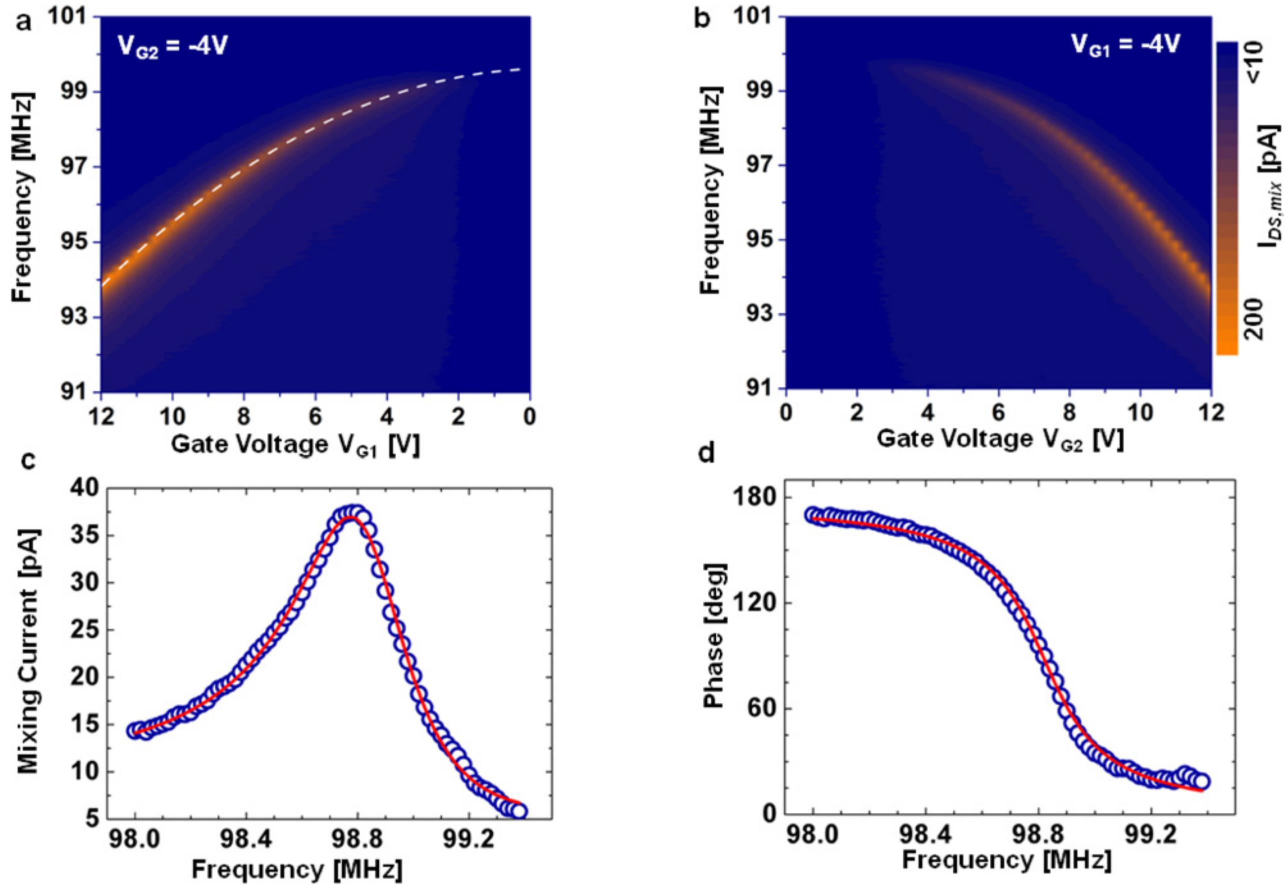

Fig. 5. **Open-loop response in high vacuum and at room temperature. a,** Contour plot showing the mechanical resonance of the 1.7 μm long nanowire as a function of gate voltage V_{G1} in steps of 250 mV (V_{G2} = -4V, P_{drive} = -38 dBm, P_{bias} = -36 dBm). The dashed line is a quadratic fit of the resonance frequency versus the gate voltage. The tuning range of the mechanical resonance is over 5% at 100 MHz. **b,** Contour plot for mirrored bias conditions, showing the mechanical resonance as function of V_{G2} in steps of 250 mV (V_{G1} = -4V). **c,** Data cut of the plot 4b corresponding to V_{G2} = +6V, showing the magnitude of $I_{DS,mix}$ versus the frequency. The red line is a Lorentzian fit, the extracted quality factor in vacuum is Q $\sim$ 342. **d,** The corresponding lock-in phase recorded versus the frequency, indicating the π-phase shift around resonance.

on/off current ratios beyond 10^6 and clear exponential dependence in sub-threshold. The inset of Fig. 4a shows the device transfer characteristic when using the two gate electrodes independently (Ref. 17). For a constant gate voltage V_{G1} = -4V, a threshold voltage of + 3V was obtained. The experimental output characteristic in Fig. 4b reveal good current saturation behaviors for higher V_D and excellent linear characteristics of I_D at low V_D. A wide selection range of bias points was obtained under which the resonant junctionless transistor can be operated.

B. Resonant Characteristics

Fig. 5a-5d show the spectral response of a nanowire resonator with a length of 1.7 um. Fig. 5a-5b are contour color plots; the frequency was scanned over a range of gate voltages. We used asymmetric gate bias conditions to detect the resonance. The fundamental, in-plane resonance appears in yellow; the blue background represents the mixing current in the absence of any mechanical displacement. The negative dispersion of the in-plane mode is a consequence of the decreasing effective spring constant for increasing gate bias. The frequency tuning of $\sim$1 MHz/V confirms the strong electrostatic coupling between the nanowire and side-gate through the lateral transduction gaps. Comparing Fig. 5a with 5b, the symmetry in the response indicates the presence of homogeneous side gate fields and high structural symmetry. The disappearance of the resonant signal for a gate voltage below $\sim$3V coincided with the transistor threshold voltage, i.e. with the current pinch-off in the silicon body, which we measured around $\sim$3V for this device under the respective bias conditions (V_{G1} = -4V) (compare with inset of Fig. 4a). This can only be understood on the basis of a current modulation mechanism resulting from the depletion charge modulation and the field effect [17]. Fig. 5c and 5d shows the magnitude and the phase of the resonance response. The red line is a fit to a Lorentzian line shape. The extracted quality factor was Q $\sim$ 342 in high vacuum and at room temperature. We measured also the response for shorter beams, with fundamental resonant frequencies detected up to 226 MHz [22].

Fig. 6 shows the typical response of the resonator as a function of frequency as the drive power is increased. The bifurcation towards higher frequencies indicates spring stiffening and the presence of mechanical nonlinearities. The nonlinear response limited the available dynamic range [23], which is defined as the ratio of the maximum amplitude with predominantly linear response to the *rms* readout noise floor.

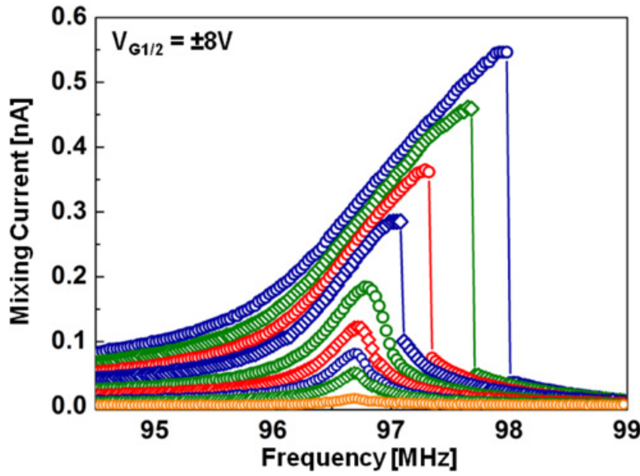

Fig. 6. **Nonlinear response of the nanowire resonator with a length of 1.7**μ m. As the drive power is increased from -46 to -22 dB ($P_{bias} = -36$ dBm), the spring stiffens, which leads to bifurcation towards higher frequencies. This is typical for a Duffing oscillator and indicates the presence of mechanical nonlinearities.

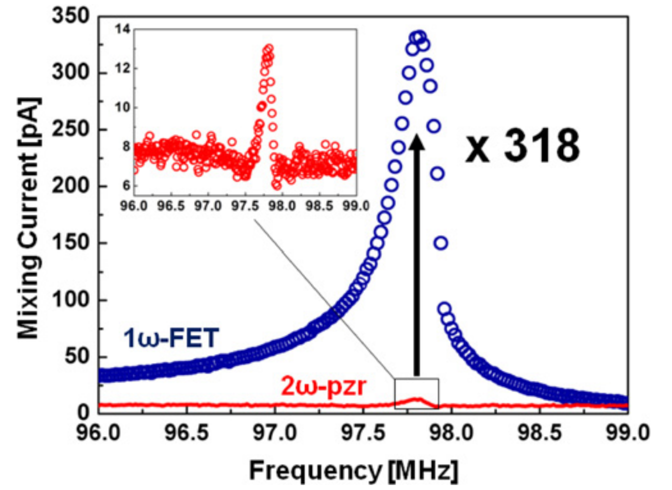

Fig. 7. **SNR-enhancement with 1**ω**-field-effect detection.** The resonance detection is compared using the 1ω-field-effect (blue curve) versus the 2ω-piezoresistive (red curve) current modulation. The dc bias is $V_{G1/2} = \pm 7$V and $V_{G1/2} = +7$V, respectively. The resonant response stems from the same device under the same ac drive conditions (P_{drive} = -40 dBm and P_{bias} = -26 dBm).The 1ω-field-effect detection offers an increase of $\sim$50 dB in signal output and of $\sim$27 dB in signal-to-background. The resonator has a length of 1.7 μm.

Under optimized bias conditions, up to $\sim$ 45 dB dynamic range were achieved.

A necessary condition for our detection scheme, which we called the 1ω-field-effect detection, is the asymmetric gate bias (in magnitude and polarization). In fact, for a symmetric field distribution, the resonance could be detected because the conductance modulation due to the field effect was symmetric with respect to the neutral axis. A similar argumentation followed for the first-order piezoresistance, which canceled out due to symmetry in the cross-section. Under symmetric bias conditions, the resonance can only be detected *via* the second-order piezoresistance, initially proposed by He *et al.* [13]._ENREF_13 In this case, the non-vanishing longitudinal strain is exploited, which has quadratic dependence on the displacement. The piezoresistive modulation, which in this case occurs twice per cycle of vibration, is described by:

$$\frac{\Delta G}{G_0} = K\varepsilon_y \tag{4}$$

where ΔG is the strain induced conductance change, G_0 the static conductance of the nanowire, K the piezoresistive gauge factor, and ε_y the axial strain. For the 2ω-piezoresistive modulation, we modified our detection circuit of Fig. 3 according to the setup reported in Ref. [13] in combination with a frequency doubler (FDS6005 by Teledyne Cougar).

We then experimentally compared the efficiency of these two detection mechanisms, within the same device and under identical drive and bias conditions (Fig. 7). The 1ω-field-effect detection yielded a $\sim$320-fold increase in signal output. This corresponded to a + 35 dB increase in SNR for this device when the depletion modulation is used instead of the 2ω-piezoresistive modulation. Three main factors could contribute to the greatly enhanced signal output: i) the second-order piezoresistance is weaker in highly doped n-type semiconductor material [24], [25], ii) the transistor, used as resistive mixer, has a higher conversion efficiency and output SNR compared to purely piezoresistive frequency down-conversion [17], and iii) the first-order piezoresistance does not completely cancel out due to the broken symmetry and can contribute to the total current modulation.

We estimated and compared the nanowire conductance change for different modulation mechanisms (calculations described in Appendix A). The displacement at the center of the 1.7 μm long resonator was estimated $\sim$ 4.5 nm at onset to mechanical nonlinearity (see Fig. 6) [26]. The nanowire conductance in the point of operation ($V_{G1/2} = \pm 8$V) was typically $G_0 \sim 0.51\,\mu$S and was obtained from static measurements. This resulted in a motion induced conductance change owing to the field effect of ΔG $\sim$ 63 nS, or $\Delta G/G_0 \sim 12.4 \times 10^{-2}$. The second-order strain was about $\varepsilon_l \sim 1.7 \times 10^{-5}$. The Gauge factor of $K \approx$ *-52* was taken from previous work [25], [27]. This resulted in a second-order piezoresistive modulation, which was in the order of $\Delta G/G_0 \sim 9\times10^{-4}$, close to the value reported in [13]. For comparison, the strain generated by the bending moment was about $\varepsilon_b \sim 4.5\times10^{-4}$, one order of magnitude larger that the second-order strain. The maximal possible signal due to the first-order piezoresistance modulation was then estimated $\Delta G/G_0 \sim 2.4\times10^{-2}$ [24].

The above estimations indicate that the depletion charge modulation can be orders of magnitude stronger compared to the second-order piezoresistive effect. Importantly, through the control of the depletion charge, it becomes principally possible to collect the strain of the same sign and exploit the first-order piezoresistance, which can significantly contribute to the overall modulation of the drain current. As such, the proposed depletion charge modulation stands as unique versatile device for comparing the field effect and the piezoresistive modulation efficiency in the same structure, depending on size and doping. It remains important for both understanding the physics of the device and for optimizing the resonator electrical characteristics for future integrated read-out schemes.

C. Frequency Stability

Many applications based on nanomechanical resonators require monitoring the natural frequency of oscillation over time with high precision. The short term stability of the mechanical oscillation directly benefits from an increased output SNR, as both are inversely related to each other [28], [29]:

$$\frac{\partial f}{f_0}(\tau) \propto \frac{1}{Q}\frac{\tau^{-1/2}}{SNR}(5) \quad (5)$$

where τ is the integration time. We integrated our device into a digital feedback loop which tracked the resonance frequency in real-time (Fig. 8a). This allowed us to measure the *rms* fractional frequency fluctuations. Fig. 8b (left axis) shows the experimental frequency stability $\langle \delta f \rangle$ of the 97 MHz resonator, measured both in high vacuum and at ambient conditions. In vacuum, the instability could be reduced to ~1 kHz (or 10 ppm) by increasing the integration time to $\tau = 5$s. In air, the reduced quality factor of Q $\approx$ 80 deteriorated the frequency stability. However, the higher applicable input drive (and thus mixing output SNR) partially compensated for the Q-reduction and excellent frequency stability (~20 ppm) at ambient could be achieved. For shorter integration times (< 5s), the stability scaled with $\delta f \sim \tau^{-1/2}$ according to equation (5), for medium integration times the signal seemed 1/f-noise limited ($\delta f \sim \tau^0$). For longer time intervals (> 50s), random walk ($\delta f \sim \tau^{1/2}$) deteriorated the stability. We note that equation (5) can be used to crudely predict the frequency stability based on separately measurable parameters (Q, SNR). For input drives well below mechanical nonlinearity and short integration times (~1s), the calculated stability values agreed reasonably well experimental values (~15 % error). For higher input drives, we found that the calculated values consistently overestimated the frequency stability.

One promising application based on NEMS is their use as gravimetric sensor, offering an unprecedented mass sensitivity. The frequency noise floor translates into an equivalent mass noise floor, $\langle \triangle M \rangle \approx 2M_{\mathrm{eff}}\langle \delta f/f_0 \rangle$. The modal mass was determined through careful inspection of the resonator geometry and cross-sectional dimensions in conjunction with the analytical expression of M_{eff} for the doubly-clamped beam in its fundamental mode and point mass loading at the center of the beam. We estimated $M_{\mathrm{eff}} = 0.4M_{\mathrm{total}} \approx 5.4$ fg. The corresponding mass detection noise floor (in kilo-Dalton, 1 kDa $\approx 1.66\times10^{-21}$ g) is shown in Fig. 8b (right axis). Assuming a practical SNR of 3:1, we found the minimum resolvable mass of $\triangle M_{\mathrm{min}} \approx 180$ kDa at 300 K in high vacuum. For comparison, the molecular weight of *Bovine Serum Albumin*, a biological macro-molec_ENREF_25ular assembly, is ~ 66 kDa, and the weight of a 5 nm gold nano particle in the MDa range [12]. This clearly highlights the use of the depletion charge modulation as a NEMS transducer, opening detection capabilities down to a individual nano particles and single molecules. We expect further improvement of the frequency stability by at least one order of magnitude by co-integration with readout electronics [20], by Q-factor engineering [30], optimization the transistor gain [16], [31], differential readout_ENREF_27_ENREF_27 [32], or reducing the temperature of operation [4], [9]. This could offer

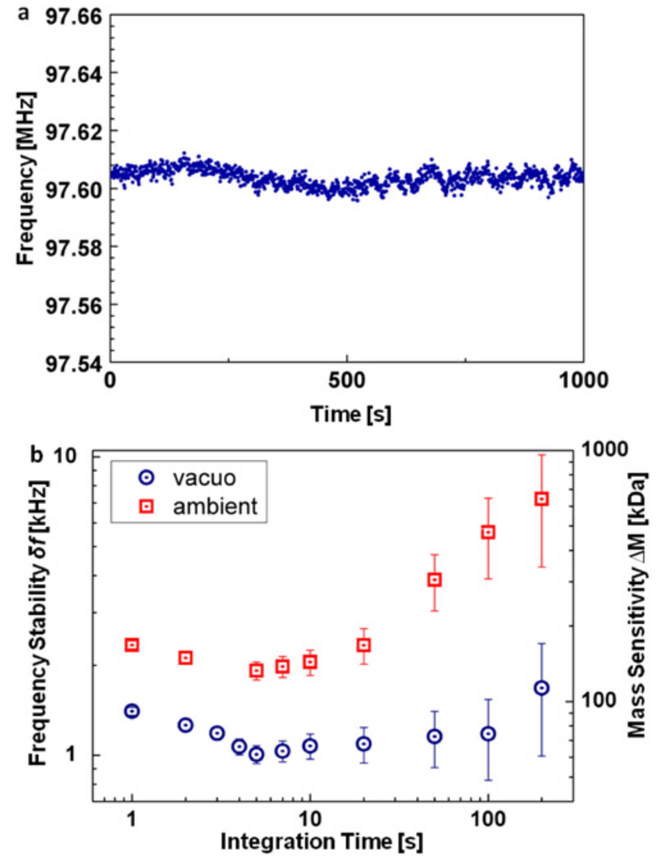

Fig. 8. **Closed-loop operation of the 98 MHz nanowire resonator at room-temperature. a,** Real-time frequency tracking, showing the resonance frequency recorded over time (in vacuum, $\tau = 1$s). The bias conditions are $V_{G1/2} = \pm 7$V, $P_{\mathrm{bias}} = -32$ dBm, $P_{\mathrm{drive}} = -46$ dBm. **b,** The frequency stability and predicted mass sensitivity as function of the integration time, in vacuum and in air. The 1ω-field-effect detection is used. Under optimized bias conditions ($V_{G1/2} = \pm 7$V, $P_{\mathrm{bias}} = -32$ dBm, $P_{\mathrm{drive}} = -46$ dBm), the Allan deviation can be reduced to 10 *ppm* for 5s integration time in vacuum, which corresponds to a mass noise floor of ~ 60 kDa. At ambient, the resonator is driven harder ($V_{G1/2} = \pm 10$V, $P_{\mathrm{bias}} = -32$ dBm, $P_{\mathrm{drive}} = -20$ dBm), reaching a frequency stability of ~ 20 ppm.

detection capabilities in the low kDa range combined with all the benefit of conventional, large-area technology. So far, this detection range has been only accessed by bottom-up devices [1], [6], [7], [13], [33], [34]. Large arrays of resonators remain essential to enhance the robustness, the signal-to-noise [35] and the capture cross section of nano sensors [36].

VI. Outlook

In this letter, we exploited the depletion charge modulation in a junctionless, suspended-channel FET to transduce the mechanical oscillation of sub-40 nm n + silicon nanoelectromechanical resonators on-chip. A large range of dc bias points can be selected to operate the resonant nanowire transistor. This electromechanical transducer is suited for a class of ultra-thin silicon resonators, and not limited by further dimensional scaling. The detection mechanism can offer a substantial improvement in the output signal-to-noise compared to the second-order piezoresistive modulation, measured within the same device. The full control of the depletion charge within

the silicon body further offers a means to compare, or even to combine, the field effect and the piezoresistive modulation in resonant nano structures, depending on size and doping. In broader terms, our results demonstrate that the concepts and the technologies that primarily advance the continued scaling of solid-state FETs [37] can be readily applied to integrate NEMS. Interfaced with advanced CMOS on a single silicon chip, such devices can be used in collective electromechanical signal processing based on millions of resonant transistors. This brings new opportunities for More-than-Moore systems, offering a wide range of applications from analog, RF to ultra-sensitive sensing.

VII. Appendix A

In the triode region ($V_G >> V_{th}$, $V_D << V_G - V_{th}$), the FET current-voltage characteristics are linearly approximated:

$$I_D \cong \frac{\mu}{L_{ch}^2} C_g V_D V_G \tag{1A}$$

$$g_m = \frac{\partial I_D}{\partial V_G} \cong \frac{\mu}{L_{ch}^2} C_g V_D \tag{2A}$$

The nanowire conductance G_0 in the respective transistor point of operation ($V_{G1/2} = \pm 8V$) was obtained from static measurements in conjunction with the relation $I_D = f(V_D)$ of eq. A1, yielding $G_0 \sim 0.51\,\mu S$. Similarly, by evaluating the relation $g_m = f(V_D)$ in eq. A2, the bulk electron mobility was extracted to $\mu \sim 123..166\,cm^2/Vs$.

The gate capacitance was evaluated as $1/C_g = 2/C_{ox} + 1/C_{gap} \approx 1/C_{gap}$. The depletion capacitance was neglected. For the gap-capacitance, the fringing fields were included by using the Palmer approximation (H. B. Palmer, Trans. AIEE 56, pp. 363, 1927). Its derivative with respect to the displacement was

$$\frac{\partial C_g}{\partial z} \cong C_g \left(\frac{1}{gap} + \frac{1}{\pi T} \right) \tag{4A}$$

where T is the total device layer thickness.

The critical displacement amplitude was estimated [26]

$$z_{cr} \cong \frac{W}{\sqrt{0.53 Q \left(1 - \nu^2\right)}} \tag{5A}$$

where W is the total resonator width and ν the effective Poisson ratio ($\nu \sim 0.144$). Alternatively, the displacement was estimated by evaluating Fig. 6 in conjunction with the expression

$$z \cong \frac{\partial C_g}{\partial z} \frac{\tilde{v}_g V_G Q}{\omega_0^2 m_{eff}} \tag{6A}$$

We obtained reasonable agreement between eq. A5 and eq. A6, with an estimated displacement amplitude about $\sim 4.5\,nm$ at onset of mechanical nonlinearity (at the respective drive power of -30 dBm or 14 mVrms).

The change in conductance due to the displacement and the field effect in a resonant-body FET is [6], [17]:

$$\Delta G \cong \frac{\mu}{L_{ch}^2} C_g \left[\left(\frac{1}{gap} + \frac{1}{\pi T} \right) z_{cr} V_G + \tilde{v}_g \right] \tag{7A}$$

where the term outside of the bracket was evaluated from static measurements in conjunction with eq. A2. The change in conductance due to the field effect modulation was estimated in the order of 63 nS, or 12 %.

The first-order strain caused by the bending moment was estimated according to [16]

$$\varepsilon_b \cong 16 z_{cr} \frac{W_{si} - W_{depl}}{L^2} \tag{8A}$$

The piezoresistive modulation is effective only if the strain of the same sign can be collected (compressive or tensile), i.e. for $W_{depl} \geq 0.5\,W_{si}$. The best case value $\varepsilon_{b,\ max}$ is then for $W_{depl} = 0.5\,W_{si}$. The relative conductance change was then estimated up to $\triangle G/G_0 = K \cdot \varepsilon_{b,max} \approx 2.4\%$.

The Gauge factor was assumed $K = E_{110}\ \pi_l \approx -52$, with $E_{110} \sim 169$ GPa being the Young's module and $\pi_l \sim -31 x 10^{-11}$ Pa the longitudinal piezoresistive coefficient [25], [27]. The modulation due to the second-order strain was evaluated $\triangle G/G_0 = K \cdot \varepsilon_l \approx 0.09\%$. The strain is related to the square of the displacement, and estimated according to $\varepsilon_l \cong 2.44 (z_{cr}/L)^2$, where L is the total resonator length.

We note that the piezoresistive contributions remain strongly estimative considering the experimental uncertainty of the Gauge factor and the exact distribution of the depletion charge in the silicon nanowire.

Acknowledgment

The authors would like to thank E. Ollier and C. Dupre (CEA-LETI Grenoble, France), partner of the FP7 European project NEMSIC (Grant 224525), for fabrication of the device, and A. Rusu, D. Grogg, and D. Tsamados for helpful discussions.

References

[1] J. Chaste, A. Eichler, J. Moser, G. Ceballos, R. Rurali, and A. Bachtold, "A nanomechanical mass sensor with yoctogram resolution," *Nat. Nanotechnol.*, vol. 7, no. 5, pp. 301–304, Apr. 2012.

[2] H. J. Mamin and D. Rugar, "Sub-attonewton force detection at millikelvin temperatures," *Appl. Phys. Lett.*, vol. 79, no. 20, pp. 3358–3360, Nov. 2001.

[3] J. D. Teufel, T. Donner, D. L. Li, J. W. Harlow, M. S. Allman, K. Cicak, *et al.*, "Sideband cooling of micromechanical motion to the quantum ground state," *Nature*, vol. 475, no. 7356, pp. 359–363, 2011.

[4] M. S. Hanay, S. Kelber, A. K. Naik, D. Chi, S. Hentz, E. C. Bullard, *et al.*, "Single-protein nanomechanical mass spectrometry in real time," *Nat. Nanotechnol.*, vol. 7, no. 9, pp. 602–608, Sep. 2012.

[5] J. W. Ndieyira, M. Watari, A. D. Barrera, D. Zhou, M. Vogtli, M. Batchelor, *et al.*, "Nanomechanical detection of antibiotic mucopeptide binding in a model for superbug drug resistance," *Nat. Nanotechnol.*, vol. 3, no. 11, pp. 691–696, 2008.

[6] V. Sazonova, Y. Yaish, H. Ustunel, D. Roundy, T. A. Arias, and P. L. McEuen, "A tunable carbon nanotube electromechanical oscillator," *Nature*, vol. 431, no. 7006, pp. 284–287, 2004.

[7] C. Y. Chen, S. Rosenblatt, K. I. Bolotin, W. Kalb, P. Kim, I. Kymissis, *et al.*, "Performance of monolayer graphene nanomechanical resonators with electrical readout," *Nat. Nanotechnol.*, vol. 4, no. 12, pp. 861–867, Sep. 2009.

[8] K. L. Ekinci and M. L. Roukes, "Nanoelectromechanical systems," *Rev. Sci. Instrum.*, vol. 76, no. 6, pp. 061101-1–061101-12, 2005

[9] Y. T. Yang, C. Callegari, X. L. Feng, K. L. Ekinci, and M. L. Roukes, "Zeptogram-scale nanomechanical mass sensing," *Nano Lett.*, vol. 6, no. 4, pp. 583–586, Apr. 2006.

[10] M. Li, H. X. Tang, and M. L. Roukes, “Ultra-sensitive NEMS-based cantilevers for sensing, scanned probe and very high-frequency applications,” *Nat. Nanotechnol.*, vol. 2, no. 2, pp. 114–120, 2007.

[11] J. M. Rothberg, W. Hinz, T. M. Rearick, J. Schultz, W. Mileski, M. Davey, *et al.*, “An integrated semiconductor device enabling non-optical genome sequencing,” *Nature*, vol. 475, no. 7356, pp. 348–352, Jul. 2011.

[12] A. K. Naik, M. S. Hanay, W. K. Hiebert, X. L. Feng, and M. L. Roukes, “Towards single-molecule nanomechanical mass spectrometry,” *Nat. Nanotechnol.*, vol. 4, no. 7, pp. 445–450, 2009.

[13] R. R. He, X. L. Feng, M. L. Roukes, and P. D. Yang, “Self-transducing silicon nanowire electromechanical systems at room temperature,” *Nano Lett.*, vol. 8, no. 6, pp. 1756–1761, 2008.

[14] E. Mile, G. Jourdan, I. Bargatin, S. Labarthe, C. Marcoux, P. Andreucci, *et al.*, “In-plane nanoelectromechanical resonators based on silicon nanowire piezoresistive detection,” *Nanotechnol.*, vol. 21, no. 16, p. 165504, Apr. 2010

[15] J. P. Colinge, C. W. Lee, A. Afzalian, N. D. Akhavan, R. Yan, I. Ferain, *et al.*, “Nanowire transistors without junctions,” *Nat. Nanotechnol.*, vol. 5, no. 3, pp. 225–229, 2010.

[16] D. Grogg and A. M. Ionescu, “The vibrating body transistor,” *IEEE Trans. Electron. Dev.*, vol. 58, no. 7, pp. 2113–2121, Jul. 2011.

[17] S. T. Bartsch, A. Lovera, D. Grogg, and A. M. Ionescu, “Nanomechanical silicon resonators with intrinsic tunable gain and sub-nw power consumption,” *ACS Nano*, vol. 6, no. 1, pp. 256–264, 2012.

[18] D. Weinstein and S. A. Bhave, “The resonant body transistor,” *Nano Lett.*, vol. 10, no. 4, pp. 1234–1237, 2010.

[19] N. Abele, R. Fritschi, K. Boucart, F. Casset, P. Ancey, and A. M. Ionescu, “Suspended-gate MOSFET: Bringing new MEMS functionality into solid-state MOS transistor,” in *Proc. Int. Electron. Devices Meeting*, 2005, pp. 1075–1077.

[20] E. Ollier, C. Dupre, G. Arndt, J. Arcamone, C. Vizioz, and L. Duraffourg, *et al.*, “Ultra-scaled high-frequency single-crystal si NEMS resonators and their front-end co-integration with cmos for high sensitivity applications,” in *Proc. IEEE 25th Int. Conf. MEMS*, 2012, pp. 1368–1371.

[21] S. T. Bartsch, A. Rusu, and A. M. Ionescu, “Phase-locked loop based on nanoelectromechanical resonant-body field effect transistor,” *Appl. Phys. Lett.*, vol. 101, no. 14, pp. 153116–153116-5, Oct. 2012.

[22] M. U. Demirci and C. T. C. Nguyen, “Higher-mode free-free beam micromechanical resonators,” in *Proc. IEEE Int. Freq. Control Symp. PDA Exhibit. Joint. 17th Eur. Freq. Time Forum*, 2003, pp. 810–818.

[23] H. W. C. Postma, I. Kozinsky, A. Husain, and M. L. Roukes, “Dynamic range of nanotube- and nanowire-based electromechanical systems,” *Appl. Phys. Lett.*, vol. 86, no. 22, pp. 223105–223105-3, May 2005.

[24] J. A. Harley and T. W. Kenny, “1/f noise considerations for the design and process optimization of piezoresistive cantilevers,” *J. Microelectromech. Syst.*, vol. 9, no. 2, pp. 226–235, Jun. 2000.

[25] Y. Kanda, “Piezoresistance effect of silicon,” *Sensors Actuators A Phys.*, vol. 28, no. 2, pp. 83–91, 1991.

[26] H. A. C. Tilmans, M. Elwenspoek, and J. H. J. Fluitman, “Micro resonant force gauges,” *Sensors Actuators A Phys.*, vol. 30, nos. 1–2, pp. 35–53, 1992.

[27] J. S. Milne, A. C. H. Rowe, S. Arscott, and C. Renner, “Giant piezoresistance effects in silicon nanowires and microwires,” *Phys. Rev. Lett.*, vol. 105, no. 22, pp. 226802–226806, 2010.

[28] K. L. Ekinci, Y. T. Yang, and M. L. Roukes, “Ultimate limits to inertial mass sensing based upon nanoelectromechanical systems,” *J. Appl. Phys.*, vol. 95, no. 5, pp. 2682–2689, Mar. 2004.

[29] K. L. Ekinci, X. M. H. Huang, and M. L. Roukes, “Ultrasensitive nanoelectromechanical mass detection,” *Appl. Phys. Lett.*, vol. 84, no. 22, pp. 4469–4471, May 2004.

[30] K. Wang, A. C. Wong, and C. T. C. Nguyen, “VHF free-free beam high-Q micromechanical resonators,” *J. Microelectromech. Syst.*, vol. 9, no. 3, pp. 347–360, Sep. 2000.

[31] N. Abele, V. Pott, K. Boucart, E. Casset, K. Segueni, P. Ancey, *et al.*, “Comparison of RSG-MOSFET and capacitive MEMS resonator detection,” *Electron. Lett.*, vol. 41, no. 5, pp. 242–244, Mar. 2005.

[32] X. L. Feng, C. J. White, A. Hajimiri, and M. L. Roukes, “A self-sustaining ultrahigh-frequency nanoelectromechanical oscillator,” *Nat Nanotechnol.*, vol. 3, no. 6, pp. 342–346, 2008.

[33] X. L. Feng, R. R. He, P. D. Yang, and M. L. Roukes, “Very high frequency silicon nanowire electromechanical resonators,” *Nano Lett.*, vol. 7, no. 7, pp. 1953–1959, 2007.

[34] J. Cao and A. M. Ionescu, “Study on dual-lateral-gate suspended-body single-walled carbon nanotube field-effect transistors,” *Solid State Electron.*, vol. 74, pp. 121–125, Aug. 2012.

[35] I. Bargatin, E. B. Myers, J. S. Aldridge, C. Marcoux, P. Brianceau, L. Duraffourg, *et al.*, “Large-scale integration of nanoelectromechanical systems for gas sensing applications,” *Nano Lett.*, vol. 12, no. 3, pp. 1269–1274, Mar. 2012.

[36] P. E. Sheehan and L. J. Whitman, “Detection limits for nanoscale biosensors,” *Nano Lett.*, vol. 5, no. 4, pp. 803–807, 2005.

[37] W. Lu, P. Xie, and C. M. Lieber, “Nanowire transistor performance limits and applications,” *IEEE Trans. Electron. Dev.*, vol. 55, no. 11, pp. 2859–2876, Nov. 2008.

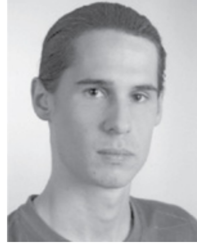

Sebastian T. Bartsch received the *Diplom-Ingenieur* degree (with distinction) in microelectronics and nanotechnology from the Technical University of Ilmenau, Ilmenau, Germany, in 2009. He completed the Diploma thesis on THz transistors at the University of California (UC), Santa Barbara, CA, USA, in 2009, after one year of graduate studies in applied physics at UC, Davis, CA, USA, as a Fulbright Fellow from 2007 to 2008. He was also awarded with the German National Academic Foundation fellowship from 2006 to 2009. He is currently a Doctoral Assistant with the Nanoelectronic Devices Laboratory, Lausanne, Switzerland. His current research interests include the design, fabrication and integration of micro- and nanoelectromechanical systems for advanced sensing and signal processing applications.

Maren Arp received the B.Sc. degree in electrical engineering and information technology from the Karlsruhe Institute of Technology (KIT), Karlsruhe, Germany, in 2011. As an Erasmus exchange student, she did graduate studies from the Swiss Federal Institute of Technology, Lausanne, Switzerland, in 2011-12, where she also joined the Nanoelectronic Devices Laboratory as a Research Assistant. She is now with KIT and pursuing the M.Sc. degree. Her current research interest include microsystems and biomedical devices to sensor-actuator systems.

Adrian M. Ionescu received the B.S. and M.S. degrees from the Polytechnic Institute of Bucharest, Bucharest, Romania, in 1989 and 1994, respectively, and the Ph.D. degree from the National Polytechnic Institute of Grenoble, Grenoble, France, in 1997. He has held Staff and Visiting positions with the Atomic Energy Commission Electronics and Information Technology Laboratory, Grenoble, with the Laboratoire de Physique des Composants à Semiconducteurs, Ecole Nationale Supérieure d’Electronique et de Radioélectricité de Grenoble, Grenoble, and with Stanford University, Stanford, CA, USA. He is currently an Associate Professor with the Swiss Federal Institute of Technology, Lausanne, Switzerland. He is also currently the Director with the Laboratory of Micro/Nanoelectronic Devices and the Head of the Doctoral School in Microsystems and Microelectronics, EPFL. He is the author of over 250 articles in international journals and conferences.

Dr. Ionescu was a member of the technical committees of IEEE Electronic Devices Meeting and was the Technical Program Committee Chair of the European Solid-State Device Research Conference in 2006. He has been appointed as the National Representative of Switzerland for the European Nanoelectronics Initiative Advisory Council and a member of the Scientific Committee of the Cluster for Application and Technology Research in Europe on Nanoelectronics. He is the European Chapter Chair of the International Technology Roadmap for Semiconductors Emerging Research Devices Working Group. He was the recipient of the Blondel Medal of the French Society of Electricity and Electronics for his contributions to the progress of science in electrical engineering, in 2009, three Best Paper Awards in international conferences, and the Annual Award of the Technical Section of the Romanian Academy of Sciences in 1994.